Energy dissipation and dispersion effects in granular media

Zhen Zhao and Caishan Liu[*]

State Key Laboratory for Turbulence and Complex Systems, College of Engineering, Peking University, Beijing, China 100871

Bernard Brogliato[†]

INRIA, Bipop Team-Project, Inovallée Montbonnot, 655 avenue de l'Europe, F-38334 Saint-Ismier, France

The strong interactions between particles will make the energy within the granular materials propagate through the network of contacts and be partly dissipated. Establishing a model that can clearly classify the dissipation and dispersion effects is crucial for the understanding of the global behaviors in the granular materials. For particles with rate-independent material, the dissipation effects come from the local plastic deformation and can be constrained at the energy level by using energetic restitution coefficients. On the other hand, the dispersion effects should depend on the intrinsic nature of the interaction law between two particles. In terms of a bistiffness compliant contact model that obeys the energetical constraint defined by the energetic coefficients, our recent work related to the issue of multiple impacts indicates that the propagation of energy during collisions can be represented by a distributing law. In particular, this law shows that the dispersion effects are dominated by the *relative contact stiffness and the relative potential energy* stored at the contact points. In this paper, we will apply our theory to the investigation of the wave behavior in granular chain systems. The comparisons between our numerical results and the experimental ones by Falcon *et al.*, [Eur. Phys. J. B **5**, 111 (1998)] for a column of beads colliding against a wall show very good agreement and confirm some conclusions proposed by Falcon *et al.* Other numerical results associated with the case of several particles impacting a chain, and the collisions between two so-called solitary waves in a Hertzian type chain are also presented.

PACS number(s): 45.05.+x, 46.40.−f, 45.70.−n

I. INTRODUCTION

Granular materials suffering shocks exhibit complex behaviors [1–5]. In particular, some ordered phenomena such as so-called "solitary wave" in one-dimensional (1D) chain systems [6–30], different pattern formation in vibrated layers [2,31–35], as well as the collective behaviors in elongated particles [20,36–40], could be observed if the microscopic properties of particles are appropriate. Yet understanding the relationship between microscopic sizes and macroscopic behaviors in granular matters still remains a challenge in mechanics and physics due to the dissipative and dispersive nature of forces acting on the interacting grains. Part of the energy within the whole system will be dissipated due to the local interplays at the contacts, such as the plastic deformation and friction as well as the adhesive forces induced by the complex interaction with an interstitial fluid (water or air) [2,12,13,31]. Meanwhile most of it will propagate and disperse to make more particles participate into the impacts during a shock process [6,8,41]. A better and deeper understanding of the mechanisms related to the dissipation and dispersion effects of the energy is fundamental for the studies of granular matters.

It is obvious that the local contact model plays a significant role for discovering the properties of the dissipation and dispersion of the energy in granular matters. Except for friction at tangential contacts, the dissipation effects during impacts come from the local plastic deformation or the viscoelasticity of the rate-dependent materials for the normal contacts between particles [31]. In order to encompass the dissipation effects in molecular-dynamics simulations, the simplest way of addressing the specifics in the course of impacts is Newton's kinematic coefficient of restitution, which originates from the concept of a binary collision between two identical spherical particles. This method can dramatically simplify the numerical simulation for the huge-dimension granular systems because the impact process is ignored by setting the ratio between velocities after and before the collision with a fixed value [39,41]. However, the approximation often yields some nonphysical behaviors such as the inelastic collapse or the divergence of the number of collisions in a finite time due to the well-known knowledge that the value of the Newton's coefficient is not a constant. In order to consider the influence of the impact velocity on the local plastic deformation between particles, a modification could be found in recent papers [34,35] by setting the coefficient of restitution with a velocity-dependent value. Such velocity-dependent restitution coefficient models have recently shown to be important in numerical and experimental studies. However, this improvement cannot essentially reflect the dissipation mechanism during the impacts because the value of the kinematic coefficient is not only related to the local plastic deformation, but also to the couplings among various contacts.

A more direct way of modeling the effects of energy dissipation is the so-called soft-particle algorithm in molecular-dynamics simulation, in which all the forces acting on a particle from either walls or other particles or external forces, are calculated based on the positions of the particles. Once

―――――――
*liucs@pku.edu.cns

†bernard.brogliato@inrialpes.fr

the forces are found, time is advanced by the explicit integration of the corresponding Newton equations of motion. There exist various models for calculating normal contact forces: some of them based on the viscoelasticity [14,42], others on the elastoplasticity of the material properties of the contact particles [31]. The shortcomings of the soft-particle method are on one hand that many parameters are required, consequently, the simulation is impractical, and that the ordinary differential equations (ODE)-stiff problem may arise in time-scale integration. This may result in the divergence of the numerical simulation away from the realistic phenomena, and then mislead the numerical observation.

The energy dispersion is another characteristic of granular systems during impacts, and depends on the intrinsic nature of the interaction law between two particles [8]. In a uniform 1D chain system with Hertz-type interaction law, the so-called solitary wave phenomena are widely discovered in plenty of experiments [13,16,20], in which the energy within the system will be confined in an approximate fixed space with about five-particle length. For the chain with a linear elastic law, however, the dispersive effects will be enlarged in comparison with the case for nonlinear Hertz-type contact, where the initial impulsive wave will move as a spreading wave with wavelength increase and its amplitude decrease during propagation [23,29]. Moreover, the profile of the pulse generated in a granular chain will be significantly affected by the mass and the material properties of the impacting particle. For instance, the so-called solitary wave may be disintegrated into a train of waves or oscillations when ones change the impacting particle [11,12,14,19,20]. The reason for that can be attributed to the phenomena of multiple compression and/or expansion cycles or the repeating impacts appearing at the contact between the impacting particle and the chain. In fact, the relative properties among various contacts (such as the mass ratios and stiffness ratios between particles) should be responsible for the potential structures of the impulsive behavior in granular materials [6]. Therefore, an underlying physical law depending on the interaction law should be established for the energy dispersion in the granular systems, such that the reason for the formation of some ordered phenomena in granular media could be discovered.

In [6], we proposed a method for solving frictionless multiple impacts in multibody systems, in which the interaction law between particles takes the power-type form for the relationship between the acting force and the indentation. The Stronge energetic restitution coefficient [43,44] is used to describe the extent of energy dissipation for dry grains with rate-independent material (such as the stainless steel). In comparison with Newton's coefficient, which usually mixes the dissipation effects and the dispersion effects together, the energetic restitution coefficient defines the dissipation in an energy level by using a ratio between input and output energy for a single compression and/or expansion cycle. This coefficient assumes that the extent of dissipation is independent on the dynamical process of multiple impacts, thus separates the energy dissipation from the energy dispersion. The dissipated energy at a contact is obtained according to the energetical coefficient and the input energy accumulated in the compression phase, which depends on the interaction law between the particles. The dissipated energy for the con-

tact with multiple compression and/or expansion cycles at the same contact point can also be obtained by using the energetic coefficient, in which the dissipated energy in each loading and/or unloading cycle is separately calculated according to the input energy of the cycle.

The dispersion effects for particles with power-type interaction laws are also well discovered in [6] by transferring the time scale into the normal impulsive scale to describe a shock process, such as the way Darboux-Keller's method is used for the frictional collision with a single contact [5]. In particular, the theoretical analysis indicates that the evolution of the energy is dominated by a distributing law that is closely related to the relative stiffnesses and the relative potential energies stored at various contacts. This law presents a clear scenario for the dispersion effects in a shock process, and may benefit us with the understanding of the complex behaviors in granular systems. Moreover, advantages in the numerical integration could also be brought in using this model because the description of the impacts is established at the energy level. Unlike the method of so-called soft-particle algorithm where the calculation for the contact forces is needed prior to the integration of the second-order ODEs, the method proposed in [6] uses the normal impulse as an independent variable, thus avoids the problems of stiffness encountered with second-order nonlinear ODEs by various numerical schemes [45].

In this paper the theory proposed in [6] is applied to investigate the shock behavior in granular chain systems. The friction effects between particles are excluded from this paper and will be studied in the future. The effects of energy dispersion and dissipation in granular media will be emphasized. The organization is as follows: Sec. II will introduce a brief overview of the theoretical aspects. In Sec. III, we will provide a comparison between the obtained numerical results and the experiments presented in [8], in which the influence of the property of the wall on the collision, the distribution of the postimpact velocities of the beads after the collision, as well as the contact force felt at the wall will be investigated. The numerical results for the case of a Hertz-type granular chain with the collisions of two solitary waves and the one of a granular chain impacted by *n* particles will be presented in Sec. IV. Summaries and conclusions are given in the final section.

II. BRIEF INTRODUCTION OF THE MULTI-IMPACT DYNAMICS

A. The impulsive dynamics

For a granular system composed of *N* spherical particles with *s* frictionless contacts, the equations of motion take the following form if no rotational degrees of freedom is considered:

$$\mathbf{M}(\mathbf{q})\ddot{\mathbf{q}} - \mathbf{h}(\mathbf{q},\dot{\mathbf{q}},t) - \sum_{i=1}^{s} \mathbf{w}_i(q)\lambda_i = 0, \qquad (1)$$

where **q** is the coordinate set of the mass centers of the particles, $\mathbf{M}(\cdot)$ is a symmetric mass matrix, $\mathbf{h}(\cdot,\cdot,\cdot)$ contains the inertial and applied forces. For each contact point i, λ_i is

the scalar value of the normal contact forces along the common normal to the surfaces of the contacting balls. The connection between normal contact forces and the generalized forces is defined by $\mathbf{w}_i(q)$, which is related to the Jacobian matrices of the contact points [46].

The kinematic state of a contact is determined by the distance $\delta_i(\mathbf{q})$ between the contacting bodies. Clearly $\delta_i(q)$ represents the normal elastic deformation when contact is established. The relative velocity of the ith contact point is expressed as

$$\dot{\delta}_i(\mathbf{q}) = \mathbf{w}_i^T(q)\dot{\mathbf{q}}. \qquad (2)$$

For a 1D granular chain consisting of n aligned balls with respective radius r_i, $\delta_i(\mathbf{q})$ can be expressed as

$$\delta_i = (x_i + r_i) - (x_{i+1} - r_{i+1}) = q_i - q_{i+1} + (r_i + r_{i+1}), \qquad (3)$$

where x_i is the displacement of the mass center for the ball B_i, $\dot{\delta}_i > 0$ corresponds to compression phases, $\dot{\delta}_i < 0$ corresponds to expansion phases. Let $[t_0, t_f]$ denote the time interval of the impact, which can be further divided into much smaller intervals $[t_i, t_{i+1}]$. According to the Darboux-Keller model [5] (Sec. 4.2.5), an integration over $[t_i, t_{i+1}]$ has to be done in order to achieve a representation of the equations of motion at the impulse level. Thus a set of differential equations with respect to the normal impulses can be obtained,

$$\int_{t_i}^{t_{i+1}} [\mathbf{M}\ddot{\mathbf{q}} - \mathbf{h} - \mathbf{W}\lambda]dt$$
$$= \mathbf{M}[\dot{\mathbf{q}}(t_{i+1}) - \dot{\mathbf{q}}(t_i)] - \mathbf{W}[\mathbf{P}(t_{i+1}) - \mathbf{P}(t_{i+1})]$$
$$= \mathbf{M} \cdot d\dot{\mathbf{q}} - \mathbf{W} \cdot d\mathbf{P} = 0. \qquad (4)$$

The terms $\mathbf{M}$, $\mathbf{W}$ remain unchanged during the integration thanks to the assumption of constant configuration q on $[t_0, t_f]$. The vector $\mathbf{h}$ consists of finite, nonimpulsive terms and therefore vanishes by the integration (see [5], Chap. 1). The quantities $d\dot{\mathbf{q}}$ and $d\mathbf{P}$ are the changes of generalized velocities and normal impulses during $[t_i, t_{i+1}]$, respectively.

It is obvious that the normal impulses $d\mathbf{P}$ are not independent since they are changed during the same interval of time. In order to make the impact differential equations of multiple impacts solvable, a connection among the normal impulses that contains the wave effects should be discovered. Therefore, adding one way or the other some compliance effects at the contact points is necessary when dealing with multiple impacts.

B. The bistiffness compliant contact model

Establishing a realistic model for the particles in contact with each other is still a tough task. Usually, one often uses a simple relationship to relate the interaction force and the overlap between two particles, in which a contact process is characterized by compression and expansion phases [43,47]. The compression (or loading) phase corresponds to a process of transferring the external kinetic energy into the potential energy stored at the contact point, while the expansion (unloading) phase will release the potential energy to make particles generate new movements. It is obvious that there may

exist a certain dissipation of energy during a compression and/or expansion cycle. In order to consider the dissipation effects due to the plastic deformation, Lankarani and Nikravesh [44] proposed a bistiffness compliant contact model, in which different force and/or indentation relationships are adopted for the compression and expansion phases.

Let us consider the case of the interaction between two particles with a power-type law, i.e., the force and/or indentation relationship for the compression phase at the contact point j can be expressed as

$$\lambda_{c,j} = K_j(\delta_{c,j})^\eta, \qquad (5)$$

where K_j is the contact stiffness, and $\lambda_{c,j}$ is the contact force during the compression phase. The subscripts c and e represent quantities related to the compression and expansion phases, respectively. The exponent η determine the kind of contacts between bodies ($\eta = \frac{3}{2}$ is for Hertz contact, $\eta = 1$ is linear elasticity).

Let us assume the form of the interaction law is not changed even though some plastic deformation is generated in the compression phase. The force and/or indentation relationship for the expansion phase is

$$\lambda_{e,j} = \lambda_{m,j}\left(\frac{\delta_{e,j} - \delta_{r,j}}{\delta_{m,j} - \delta_{r,j}}\right)^\eta, \qquad (6)$$

where $\delta_{r,j}$ is the plastic deformation, and $\lambda_{m,j}$ and $\delta_{m,j}$ correspond to the maxima of the normal contact force and normal deformation at the end of the compression phase, which corresponds to the values when $\dot{\delta}_j = 0$. For simplicity we omit the subscript j in the following expressions.

In order to constrain the local energy loss due to the permanent plastic deformation (the undeterminate scalar δ_r) generated in the compression phase, the energetic restitution coefficient [43] is applied on the compliant contact model. The integration of expressions (5) and (6) leads to

$$W_c = \int_0^{\delta_m} \lambda_c(\delta_c)d\delta_c = \frac{1}{\eta + 1}K_j(\delta_m)^{\eta+1},$$

$$W_r = \int_{\delta_m}^{\delta_r} \lambda_e(\delta_e)d\delta_e = -\frac{1}{\eta + 1}K_j(\delta_m)^\eta(\delta_m - \delta_r). \qquad (7)$$

Based on the definition of the energetic coefficient, W_c and W_r can be connected by $e_s^2 = -W_r/W_c$, where $W_c \geq 0$ and $W_r \leq 0$. In the case of a constant e_s, we have from Eq. (7)

$$\delta_r = \delta_m(1 - e_s^2). \qquad (8)$$

The indentation δ_m corresponds to the first instant t_c such that $\dot{\delta}(t_c) = 0$, so it is not a parameter of the impact dynamics. From Eq. (8) neither is δ_r. When the energetic coefficient takes a constant value, the energetic definition defines a linear relationship between the local plastic deformation δ_r and the maximum indentation δ_m, such that the dissipation of energy is reflected in an average level.

C. The potential energy at a contact point

Since the potential energy at a contact point will be accumulated during the compression phase and released in the

expansion phase, we must calculate the potential energy in the two different processes. Let us pick a point p in the curve of the compression phase. The potential energy E_p at p is equal to the work done by the contact force along the path from start of the contact to the position p. At any instant τ during the compression process, the contact force $\lambda_c(\tau)$ can always be expressed as $\lambda_c(\tau) = \frac{dP(\tau)}{d\tau}$, in which $P(\tau)$ is the normal impulse accumulated in the time interval $[0, \tau]$ corresponding to a deformation $\delta(\tau)$. Thus, we have

$$E_p(\delta^p) = \int_0^{\delta^p} dP(\tau) \frac{d\delta(\tau)}{d\tau}. \tag{9}$$

Since $P(\tau)$ and $\delta(\tau)$ can be connected by a one-to-one mapping during the compression phases, we can use the variable $P(\tau)$ to replace $\delta(\tau)$ as the integral variable. Thus,

$$E_p(P(t)) = \int_0^{P(t)} \delta_j(P(\tau)) dP(\tau) \tag{10}$$

where $P(t)$ is the normal impulse that is needed to make the indentation change from zero to δ^p by obeying the relationship (5).

When the compression process finishes, the accumulation of energy at the contact point j will be ended, and the total accumulated potential energy can be expressed as

$$W_c(\delta_m) = \int_0^{\delta_m} \lambda_c(\delta) d\delta. \tag{11}$$

After that the potential energy will be released through an expansion phase, in which the total energy that can be recovered through the expansion phase will take the value of $e_s^2 W_c$ based on the energetical constraint.

Similarly to the compression phase, the residual potential energy for a dynamical process reaching a position R located at the expansion curve can be expressed as

$$E_R = \int_0^{P_c} \dot{\delta}(P(\tau)) dP(\tau) + \frac{1}{e_s^2} \int_{P_c}^{P_t} \dot{\delta}(P(\tau)) dP(\tau), \tag{12}$$

where P_c is the normal impulse when the compression phase finishes (so $\delta = \delta_m$), $P(\tau)$ is an integral variable that is related to the normal impulse of the contact force experiencing a time interval $[0, \tau]$ by obeying the energetic relationship defined by the compliant contact model. The proof for establishing the expression (12) can be found in [6].

The first term in Eq. (12) corresponds to the total potential accumulated in the compression phase, while the second one means that the potential energy, $\frac{1}{e_s^2} \int_{P_c}^{P_t} \dot{\delta}(P(\tau)) dP(\tau)$, has been released at position R. For a full compression and/or expansion cycle, there is $e_s^2 W_c$ potential energy to be recovered in the expansion phase. If a contact experiences a multiple loading and/or unloading cycles (a new compressional phase may restart before the expansion phase finishes), we also show in [6] that the transformation between the kinetic and potential will also obey the similar relationship expressed in Eq. (12). Each cycle will dissipate a part of the energy that is related to the restitution coefficient e_s and the potential energy at the end of each compressional phase.

D. The distributing rule for the bistiffness compliant contact model

In terms of the compliant model expressed in Eq. (6) and the scale transformation of converting the time scale into the impulse scale, it is shown in [6] that the normal contact force at the contact point j during the compression and expansion phases can always be expressed as

$$\lambda_{c,j}(P_j(t)) = (1 + \eta)^{\eta/(\eta+1)} K_j^{1/(\eta+1)} [E(P_j(t))]^{\eta/(\eta+1)}. \tag{13}$$

Since the contact forces can always be expressed as the differential of the normal impulse with respect to time, from Eq. (13) the ratios between the increments of the normal impulses among various contact points j can be expressed as

$$\frac{dP_i}{dP_j} = \gamma_{ij}^{1/(\eta+1)} (E_{ij}(P_i, P_j))^{(\eta+1)/\eta}, \quad i = 1, 2, \ldots, s, i \neq j, \tag{14}$$

when all the contact points have the same η coefficient, and where $\gamma_{ij} = K_i / K_j$ and $E_{ij} = E_i / E_j$ are related to the ratios of the contact stiffnesses and the potential energy between contact points i and j. Equation (14) reflects the distribution of the increments of normal impulses in space since dP_i and dP_j vary within the same time interval. It is clear that the mode of the potential energy accumulation (the exponent in the force and/or indentation relationship) and the relative quantities of the contact stiffness among various contacts will dominate the transformation of energy within the network of contacts.

The outcomes of the multiple impacts can be obtained by combining Eq. (14) with the impulsive differential equations (4) and selecting a normal impulse at a contact point as an independent "timelike" variable. A guideline is also proposed in [6] for the selection of the independent impulse, in which the corresponding contact point is termed as the "primary contact point." This point should correspond to the point that takes the maximum potential energy among various contacts.

Since the impulse scale is used as the independent variable, the absolute values of the contact stiffnesses are not needed for the calculation of the postimpact velocities of each particle. However, if the value of the contact stiffness K_j can be estimated effectively, the value of the contact force λ_j at the instant of $P_j(t)$ can be obtained according to the potential energy $E_j(P_j(t))$, as shown in Eq. (13). Furthermore, the time t related to the normal impulse $P_j(t)$ can also be extracted by using $t = P_j(t)/\lambda_j$. This is a postprocessing associated with the impulsive differential equations, i.e., we store the information of the potential energy at each numerical step for the ODEs, then carry out an algebraic operation to obtain the values of the contact force and the corresponding time.

The multi-impact Darboux-Keller dynamics is summarized as follows:

(1) Contact parameters: γ_{ij}, e_j, $1 \leq i \leq s$, $1 \leq j \leq s$, η ($\eta = 1$—linear stiffness—or $= \frac{3}{2}$—Hertz contact—, or other suitable values), $E_{0,j}$ for the initial precompression cases.

(2) Dynamical equation:
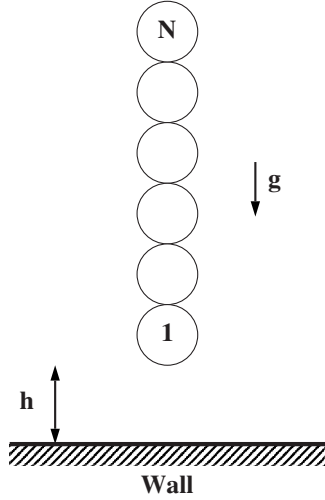
FIG. 1. A column of beads colliding against a wall.

$$\mathbf{M}\frac{d\dot{\mathbf{q}}}{dP_i} = \mathbf{W}\frac{dP}{dP_i} \quad \text{if } E_{ji}(P_j, P_i) \leq 1 \text{ for all } j \neq i \quad (15)$$

with

$$\frac{dP_j}{dP_i} = \gamma_{ji}^{1/(\eta+1)}(E_{ji}(P_j, P_i))^{(\eta+1)/\eta}, \quad (16)$$

$$E_{ji} = \frac{E_j(P_j)}{E_i(P_i)}, \quad 1 \leq i \leq s, \ 1 \leq j \leq s, \quad (17)$$

$$E_j(P_j) = E_{0,j} + \frac{1}{Tra}\int_0^{P_j(t)} \mathbf{w}_j^T \dot{\mathbf{q}} dP_j. \quad (18)$$

Tra is a parameter to transfer the work done by the normal impulse into the potential energy, in which $Tra=1$ if $\dot{\delta}>0$, and $Tra=e_j^2$ if $\dot{\delta}<0$. When $E_j(P_j(t_f))=0$ and $\dot{\delta}<0$, the contact j will be open at time $P_j(t_f)$. The details of the numerical method and its implementation are in [6].

III. THE COMPARISON BETWEEN NUMERICAL AND EXPERIMENTAL RESULTS

In this section the experimental results reported in [8] are compared to the numerical results obtained by the approach outlined in Sec. II. In [6] numerous comparisons between compliant models (Hertz or linear springs) and the Darboux-Keller model of Sec. III are presented. They already prove that the Darboux-Keller model possesses very interesting properties. The results of this section confirm these positive conclusions.

A. A column of beads colliding against a wall

Figure 1 shows the granular system studied in [8], in which N identical stainless steel beads, each one 8 mm in diameter, are put together to form a column colliding against a fixed wall. The column of beads leaves the wall with a height h and starts its free fall to collide against the wall. The

number of beads may vary from $N=1$ up to $N=40$ for experiments, and the contact forces felt at the wall are recorded by a force sensor. In order to reproduce the experimental results reported in [8], we use the bistiffness relationships expressed in Eqs. (5) and (6) to model the interactions at contacts, in which the local energy loss is taken into account by the restitution coefficient $e_{s,s}$ for particle to particle and $e_{s,p}$ for particle to wall, respectively. Let us number the contact bodies in a sequence from the wall assigned with 0 to the last bead with N. The contact points are denoted in a sequence with number 1 for the contact between the wall (0th contact body) and the 1th bead, and number N for the contact between $(N-1)$th and Nth beads. According to Hertz theory, the exponent η equals 3/2 for the nonconforming contact mode between bodies, and the contact stiffness K_i at the contact point i is expressed as

$$K_i = \frac{4}{3}R_i^{*1/2}E_i^*, \quad i = 1, \ldots, N, \quad (19)$$

where $R_i^* = \frac{R_i R_{i-1}}{R_i + R_{i-1}}$ and $\frac{1}{E_i^*} = \frac{1-\nu_{i-1}^2}{E_{i-1}} + \frac{1-\nu_i^2}{E_i}$ are the equivalent contact radius and the equivalent Young modulus between adjacent contact bodies, respectively. The mass of a stainless steel bead used in experiment is $m=2.05\times10^{-3}$ kg. The Young modulus and Poisson ratio for stainless steel are $E_s=21.6\times10^{10}$ N/m^2 and $\nu_s=0.276$, respectively. Thus, the value of the contact stiffness, K_i $(i=2,\ldots,N)$ for sphere-sphere contact is 6.9716×10^9 N/m$^{3/2}$. For the contact between the bead and the wall made of stainless steel, the value of the contact stiffness K_1 for the sphere-plane contact is 9.858×10^9 N/m$^{3/2}$.

B. The contact force felt at the wall during the collision

Based on the description in [8] for the experiments, two cases are investigated in the following numerical simulations: a column of N beads free fall to collide against the wall with two different height $h=3.1$ mm and $h=5.1$ mm, corresponding to the impacting velocities of the column $(v_{imp}=\sqrt{2gh})$ 0.246 m/s and 0.316 m/s, respectively.

For the columns of beads with N changing from 1 to 8, colliding against the wall with $h=3.1$ mm, Fig. 2 shows the outcomes of the contact forces at the wall. It is clear that our numerical results can well reproduce the experimental phenomena discovered in [8], Fig. 4a and 4b, in which the maximum force F_{max} is approximately equal to 52 N and very little influenced by N, while the duration of impact increases linearly with N. Moreover, the contact force oscillates with a period of $P\approx32$ μs (the experimental value in [8] is $P=32.4\pm1$ μs), and is damped similar to the response of the motion describing the damped free vibrations of a system with viscous damping.

Let us set the fall height $h=5.1$ mm for the column of beads with various number of $N=5,6,\ldots,12$, colliding against the wall. The numerical results obtained from our method are shown in Fig. 3, in which the maximum force F_{max} is approximately equal to 71 N and the period P for the oscillation of the contact force is around 31 μs. This also well agrees with the experimental results in [8], Fig. 4c and 4d.
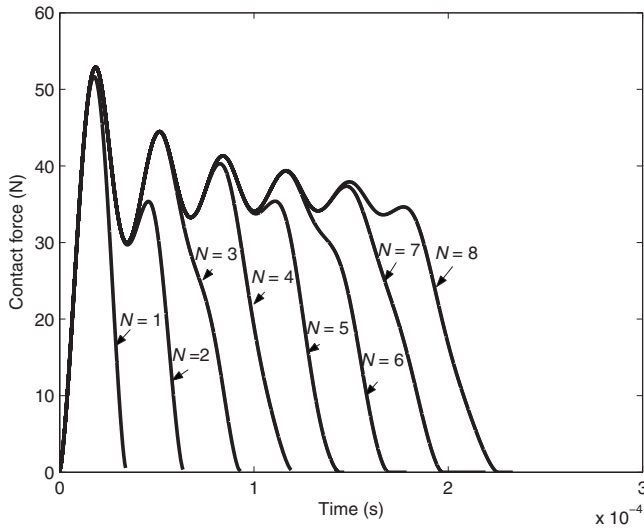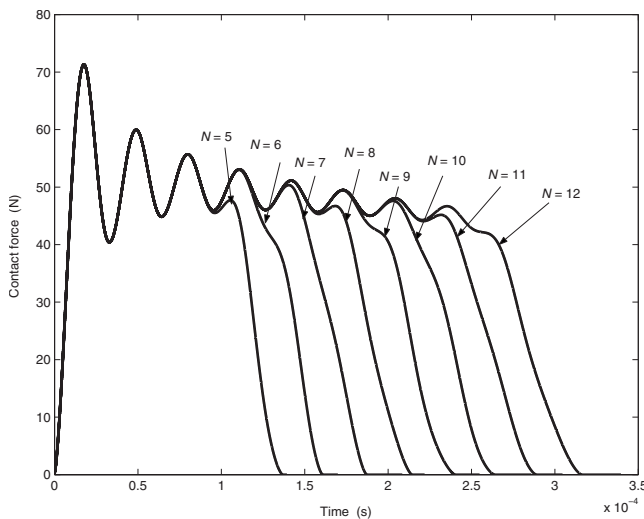
FIG. 2. The contact force at the wall during the collision of a column of $N=1,2,\ldots,8$ beads with fall height $h=3.1$ mm, $e_{s,s}=0.96$, $e_{s,p}=0.92$.
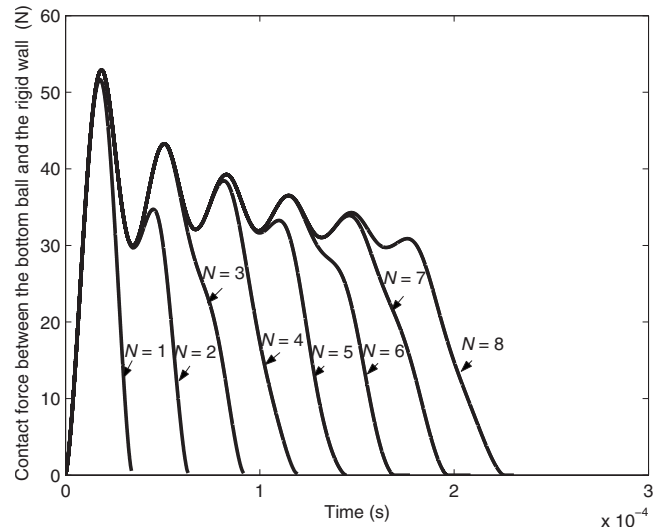

FIG. 4. The contact force at the wall during the collision of a column of $N=1,2,\ldots,8$ beads with fall height $h=3.1$ mm, $e_{s,s}=0.92$, $e_{s,p}=0.92$.

Since the value of the restitution coefficient is often estimated from an independent experiment, it may be interesting to investigate its influence on the contact force at the wall by slightly modifying e_s. Let us set both the values for particle-particle coefficient of restitution and the particle-wall one as $e_s=0.92$. Figures 4 and 5 present the numerical results for the contact forces felt at the wall that is collided by the column of beads with two different fall heights $h=3.1$ and 5.1 mm, respectively. Comparing them with Figs. 2 and 3, we find that the little change of the coefficient of restitution has no identifiable influence on the value and the shape of the curves of the contact forces at the wall. The proposed model and numerical algorithm has good robustness (insensitivity) properties.

C. Distribution of the postimpact velocities

As illustrated in [8], at the end of the collision the beads in the column will detach from each other due to the energy redistribution within the system. In this section we will apply our method to investigate the phenomena of the detachment effect found in [8,48] by presenting the postimpact velocities of the beads after the collision.

The definition of the end of the column-wall collision given in [8], in which the collision is assumed to be finished at the time at which the bead at the bottom leaves the wall, is different from ours: we use the energy calibration to define the end of the column-wall collision, corresponding to the instant when all the potential energy among various contacts is completely released. Figure 6 shows the postimpact velocities of the beads obtained from the simulation for the
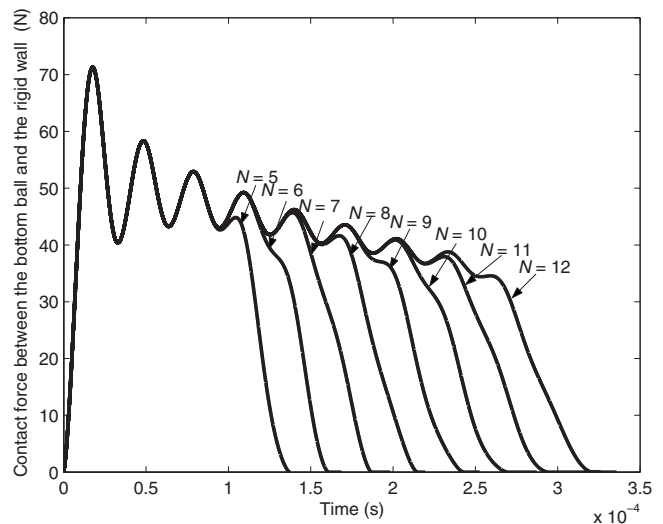

FIG. 3. The contact force at the wall during the collision of a column of $N=5,6,\ldots,12$ beads with fall height $h=5.1$ mm, $e_{s,s}=0.96$, $e_{s,p}=0.92$.

FIG. 5. The contact force at the wall during the collision of a column of $N=5,6,\ldots,12$ beads with fall height $h=5.1$ mm, $e_{s,s}=0.92$, $e_{s,p}=0.92$.
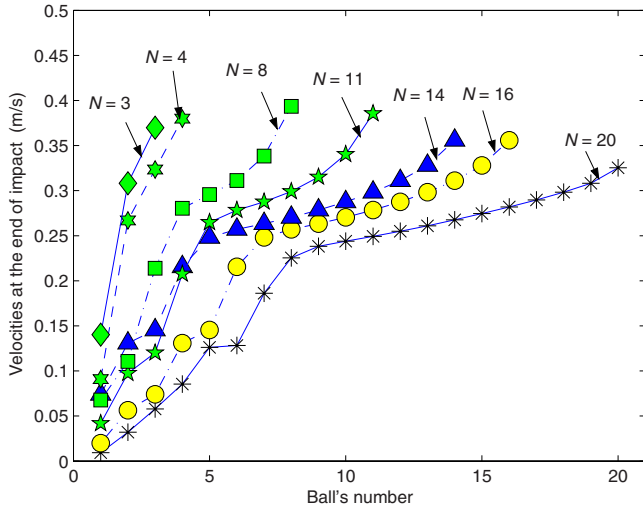
FIG. 6. (Color online) Velocity of the ith bead, at the end of the collision with fall height h=5.1 mm, as a function of the bead's number i, for different values of N=5,6,...,12 beads, and $e_{s,s}$=0.96, $e_{s,p}$=0.92.

FIG. 7. The coefficient e_{eff} for the column with different N dropped from a height h=5.1 mm, and setting $e_{s,s}$=0.96 and $e_{s,p}$=0.92.

column free falling from a height h=5.1 mm. It is clear from this figure that the upper beads of the column go away with velocities greater than v_{imp}=0.316 m/s, while the lower beads have velocities smaller than v_{imp}. Moreover, we can also find that the postimpact velocity of the last ball will increase with N, and reach the maximum value at N=8, then decrease when N is further enlarged. Unlike a uniform chain impacted by an identical particle, where a regular wave could be formed and confined within five particles, the wave behavior in the column is complex and unregular similar to the phenomena discovered in the next section, in which n-ball chains are impacted by m-ball chains (hence N=m+n). However, we can still observe the following interesting phenomena: If N<8, the beads will separate one after the other from the top of the column. For N>8, some beads separate, while others are leaving in a cluster since the discrepancies between the postimpact velocities of the beads are very small. If N>8, the local energy loss will make the postimpact velocity of the top-bead decrease. Due to the local energy loss, it is imaginable that the top bead will not bounce anymore if the column is long enough.

The *effective coefficient of restitution* for the whole chain, proposed in [48] and then applied in [8], is defined as

$$e_{eff} = \frac{\Sigma_{i=1}^{N} v_i^+}{\Sigma_{i=1}^{N} v_i^-} = -\frac{1}{N v_{imp}} \sum_{i=1}^{N} v_i^+, \qquad (20)$$

where v_i^+ corresponds to the postimpact velocity of ith beads. It is noteworthy that the value of v_i^+ is different from the one of v_i^f in [8], Eq. (7), where all the values for each v_i^f correspond to the instant when the force felt at the wall equals zero. Figure 7 presents the value of e_{eff} varying with N for a column free fall with a height h=5.1 mm. The tendency of the variation of e_{eff} agrees well with [8], Fig. 11. However, when N>4 there is an obvious discrepancy between the value of e_{eff} obtained from our numerical results and the one shown in [8], Fig. 11. This can be attributed to the different
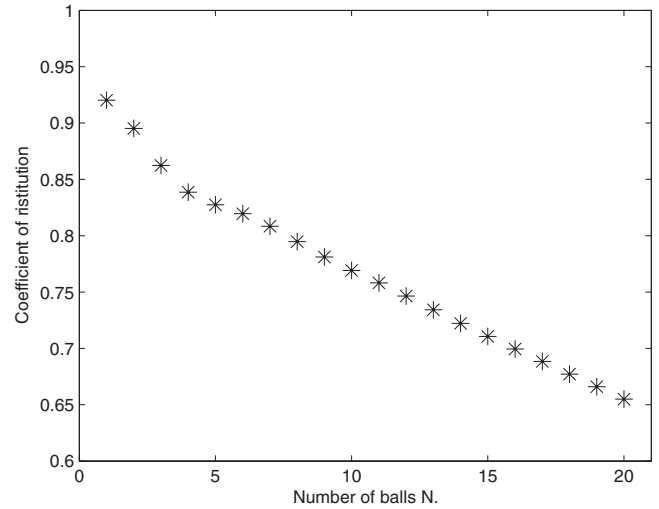
definitions for v_i^+ in the two figures for the calculation of e_{eff}.

Comparing Figs. 2 and 4, with Figs. 3 and 5, respectively, we can find that the variation of the value of the restitution coefficient $e_{s,s}$ has little influence on the value of the contact force at the wall. However, it will change the distribution of the postimpact velocities of beads (the dispersion effect) that seems not to be ignorable. Let us only change the value of $e_{s,s}$ from 0.96 to 0.92 while keeping other parameters with the same values as used for Fig. 7. We can find from Fig. 8 that the curve of e_{eff} has an identifiable variation due to the little change of $e_{s,s}$. This means that the local energy loss will influence the distribution of the postimpact velocities of the beads. This can be further confirmed by Fig. 9, in which $e_{s,s}$ is assigned as 0.7, and the effective coefficient of the whole column, e_{eff} for N=20 is near to 0.1, corresponding to the column with a small bounce.
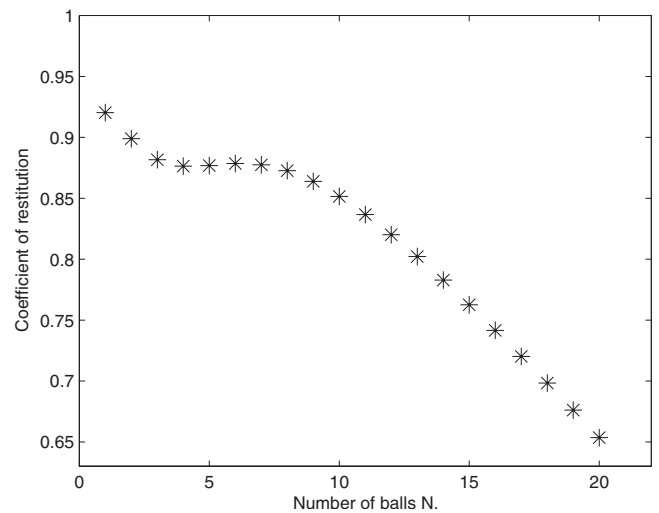

FIG. 8. The coefficient e_{eff} for the column with different N dropped from a height h=5.1 mm, and setting $e_{s,s}$=$e_{s,p}$=0.92.
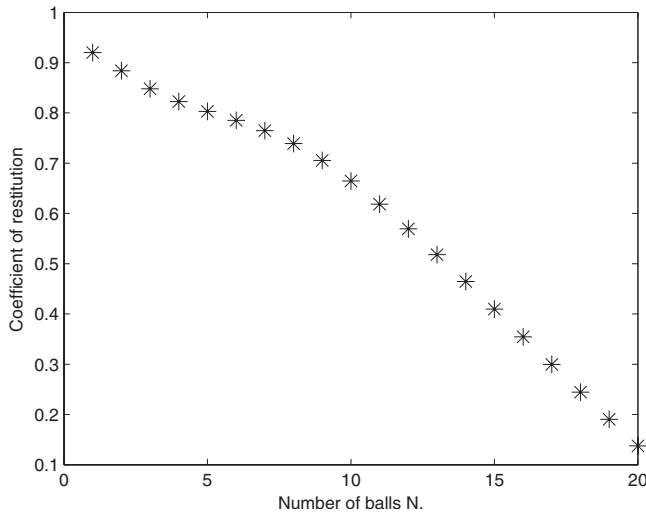
FIG. 9. The coefficient e_{eff} for the column with different N dropped from a height $h=5.1$ mm, and setting $e_{s,s}=0.7$ and $e_{s,p}=0.92$.

D. Influence of the mechanical properties of the wall

The mechanical property of the wall will significantly influence the collision processes as exhibited in [8]. Further investigations can also be found in recent studies in the physics community [12,15,16]. For instance, Job *et al.* [15] performed a precise experiment to reflect the dependence of the impulsive wave on the wall mechanical properties. Similar phenomena are also found in the experiments by Daraio and co-workers [12,13].

In [8], Falcon *et al.* carried out different experiments by setting the column of beads colliding against the wall with different materials. According to the output signal from the force sensor they found that the rigidity of the wall will influence the collision behavior. For example, experimental results show that the maximum contact force felt at the wall will depend on the number N when a soft material sheet is stuck on the sensor. Since the mechanical parameters for the materials covered in the wall are not provided in [8], we use the duration for one bead colliding with a plane to estimate the contact stiffness between the bead and the plane covered with various material. According to Hertz theory, the contact time τ_1 between a bead dropped from a height h and a plane assumed to be of infinite mass can be approximately expressed as

$$\tau_1 = 2.94 \left(\frac{5m}{4K_1} \right)^{2/5} v_{imp}^{-1/5}. \quad (21)$$

TABLE I. The value of the contact stiffness K_1 estimated from experimental results for the contact time between a bead dropped from a height h and a plane assumed of infinite mass in [8] Table 2.

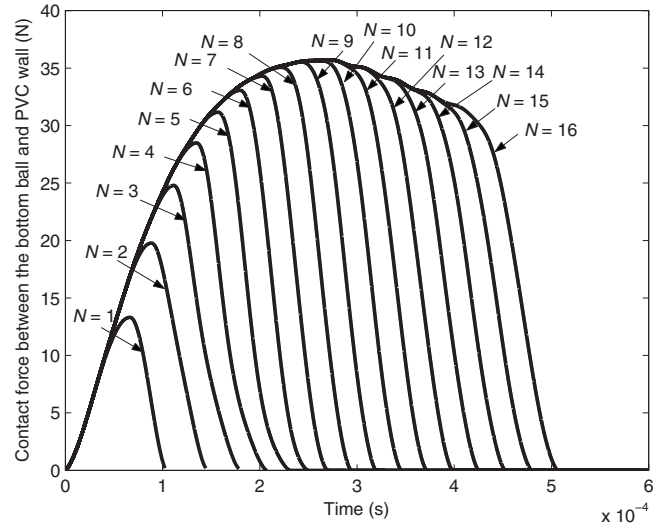| Index No.	Material	τ_{max} (s)	K_1 (N/m$^{3/2}$)
1	steel	17	1.15×10^{10}
2	PVC	67.5	3.67×10^8
3	beech	127.5	7.5×10^7
4	rubber	221	1.89×10^7

FIG. 10. The contact force at the wall with PVC during the collision of a column with $N=1,2,\ldots,16$, $h=2.9$ mm, $e_{s,s}=0.92$, $e_{s,p}=0.7$.

For a bead with mass $m=2.05 \times 10^{-3}$ kg falling from a height $h=2.9$ mm ($v_{imp}=\sqrt{2gh}=0.2385$ m/s), Table I presents the values of K_1 extracted from the $\tau_{max}(N=1)$ in [8], Table 2 and expression (21).

We can find from Table I that the value of K_1 extracted from the experiment of the stainless steel bead colliding with a stainless steel plane is larger than the theoretical value ($K_1=9.858 \times 10^9$ N/m$^{3/2}$), so it is not possible to provide a precise comparison for the contact force between our numerical results and the experimental ones in [8], Fig. 13. At best one can compare some qualitative features of the collision due to the variation of the material in the sheet.

Let us first investigate the contact force at the wall covered with polyvinyl chloride (PVC) (index 2 in Table I) by setting a column of beads with various N free falling from a height $h=2.9$ mm. From Fig. 10, the experimental phenom-
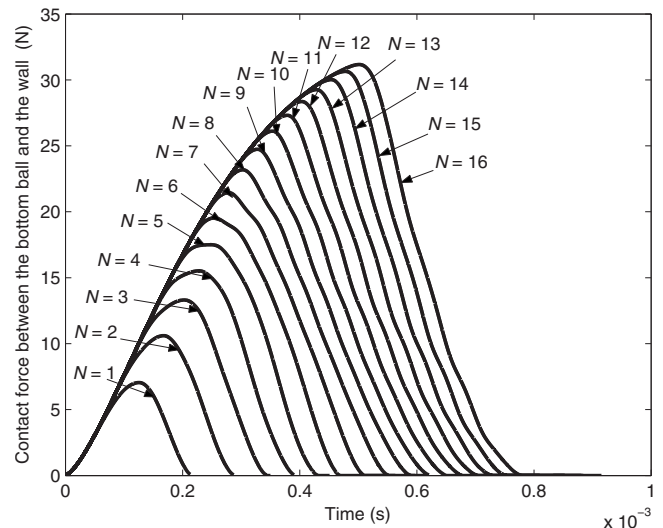

FIG. 11. The contact force at the wall with beech during the collision of a column of $N=1,2,\ldots,16$, $h=2.9$ mm, $e_{s,s}=0.92$, $e_{s,p}=0.92$.
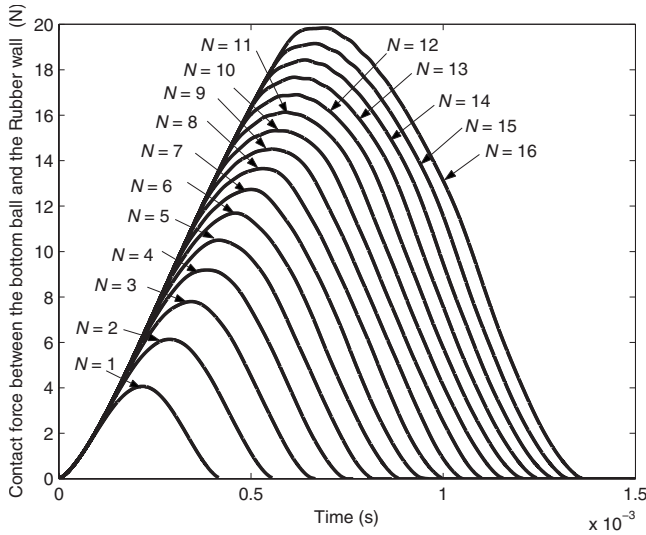
FIG. 12. The contact force at the wall with rubber during the collision of a column of $N=1,2,\ldots,16$, $h=2.9$ mm, $e_{s,s}=0.92$, $e_{s,p}=0.92$

TABLE II. The final velocities for each ball with different β. Sign "+" means "moves forward," while "−" means "moves backwards." The first figure in the last row represents the ratio between the forward postimpact kinetic energy and the total kinetic energy; the second figure is the percentage of kinetic energy in the last ball.

β	(1:9)	(2:8)	(3:7)	(4:6)
$\dot{q}_1^+$	−0.0710	−0.1126	−0.1441	−0.1706
$\dot{q}_2^+$	−0.0303	−0.0481	−0.0612	−0.0729
$\dot{q}_3^+$	−0.0159	−0.0248	−0.0312	−0.0373
$\dot{q}_4^+$	−0.0089	−0.0133	−0.0169	−0.0146
$\dot{q}_5^+$	−0.0052	−0.0068	−0.0054	0.1274
$\dot{q}_6^+$	−0.0030	−0.0022	0.0996	0.4648
$\dot{q}_7^+$	−0.0018	0.0497	0.4043	0.4847
$\dot{q}_8^+$	0.0025	0.2893	0.5108	0.9111
$\dot{q}_9^+$	0.1467	0.6570	1.0118	1.0928
$\dot{q}_{10}^+$	0.9869	1.2118	1.2323	1.2145
Percentage	(99.5, 97.4)	(99.3, 73.4)	(99.2, 50.6)	(99.2, 36.9)

ena discovered in [8] are well reproduced in our numerical results, in which the maximum force increases with N at low values of N, until it becomes independent of N, finally the contact force will slightly decrease with N similar to a damping response.

If the wall is covered with softer material, it is imaginable that the number N related to the maximum independent force will increase, and the amplitude among all the maximum forces will decrease due to the small value of the contact stiffness between the bead and the wall. Figures 11 and 12 show the results obtained from our numerical method for the column of beads with various N-chains colliding against a wall covered respectively with beech and rubber materials. The qualitative characteristics discovered in [8] are well reproduced even though the values of the contact stiffness K_1 are roughly estimated with possible large errors compared with practical situations.
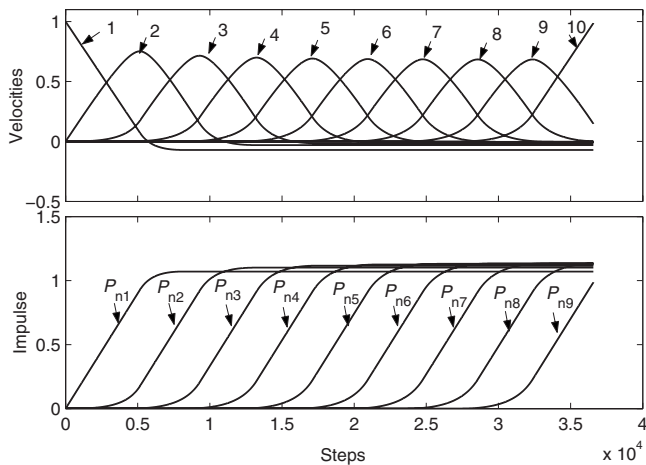
In summary, the local energy loss can be easily taken into account by using energetical constraints and the information related to the contact force and the duration of impact could also be extracted from the solutions of the differential impulsive equations through simple algebraic operations. The comparisons between our numerical results and the experimental ones in [8] show good agreement and confirm some conclusions proposed therein.

IV. OTHER NUMERICAL RESULTS RELATED TO GRANULAR CHAINS

A. *n*-ball chains impacted by *m*-ball chains

As proved theoretically and experimentally by many authors, an impulsive wave can be generated when a chain endures an impulse [7,15,16,23,25,29]. In particular, a com-
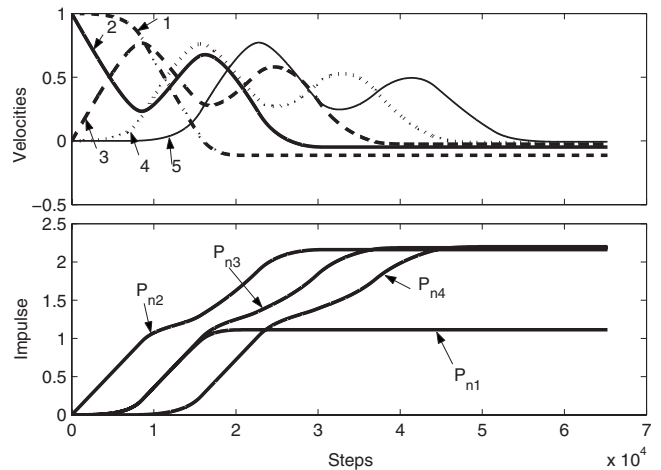

FIG. 13. The evolutions of the velocities and the normal impulses for the case of the chain with 9 particles impacted by one, $\beta=1:9$.

FIG. 14. The evolutions of the velocities and the normal impulses for a chain with eight particles impacted by two balls: β $=2:8$ (balls 1 to 5).
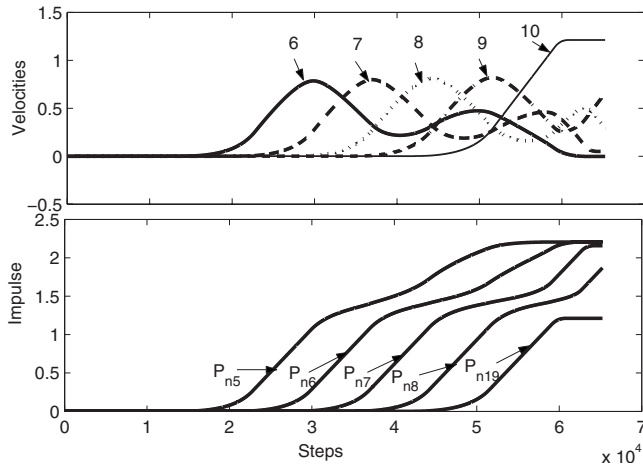
FIG. 15. The evolutions of the velocities and the normal impulses for a chain with eight particles impacted by two balls: $\beta = 2:8$ (balls 6 to 10).

pressive wave with regular profile involving five particles can be formed when a uniform ball-chain system is impacted by an identical particle. However, this regularity of the wave behavior will be destroyed when the chain is collided with by more than one impacting particles.

Let us denote a system with 10 balls that are identical and satisfy the Hertz contact relationship. The parameter β is defined as the ratio between the numbers of the m impacting balls and the n impacted balls. For instance, $\beta = 1:9$ means that the chain with nine stationary balls is impacted by one particle (i.e., $n=9$ and $m=1$), $\beta = 2:8$ is related to situation that two particles collide against eight stationary balls (i.e., $n=8$ and $m=2$), etc. We will investigate the impulsive behaviors by changing β from 1:9 to 4:6. The initial velocities of the impacting balls are set as $v_0 = 1$ m/s and no energy is dissipated during impacts: $e_{s,i} = 1$ for all contacts i.

Figure 13 presents the evolutions of the velocities and the normal impulses for the case of the chain with parameter $\beta = 1:9$. Clearly a regular wave can be formed and only three balls move forward when the impact finishes, that is near to

the half length of the wavelength. The values related to the final velocities for each ball are presented in Table II, in which the last row shows the percentages of the forward kinetic energy (the sum of the kinetic energies of the balls with positive post-impact velocity) and of the energy of the final ball with respect to the total energy of the system, respectively. In this case, the percentage of the forward kinetic energy is about 99%, and the one of the final ball is near to 97.4%.

When the chain is impacted by two identical balls, there are four balls finally moving forward, and the kinetic energy will be centralized in the last two balls. It is obvious that the wave behavior is not regular due to the complex coupling among various contacts. Figures 14 and 15 show the evolutions of the postvelocities of balls and the normal impulses for balls 1 to 5 and for balls 5 to 10, respectively. Although most of the kinetic energy of the system is still kept in the balls moving forward, the distribution of the postimpact velocities of the balls is much different from the one in the

FIG. 17. The evolutions of the velocities and the normal impulses for a chain with seven particles impacted by 3 balls: $\beta = 3:7$ (balls 6 to 10).
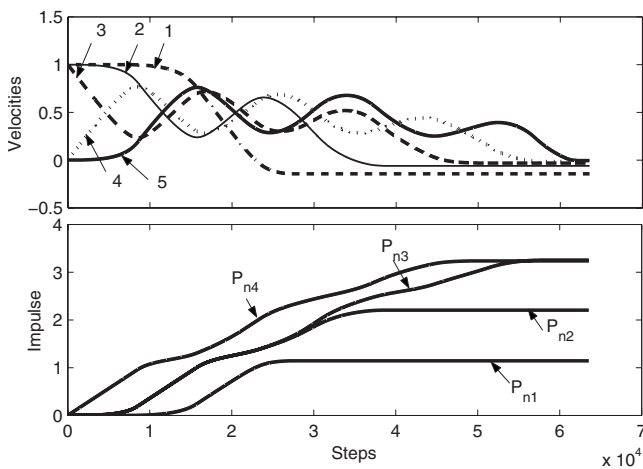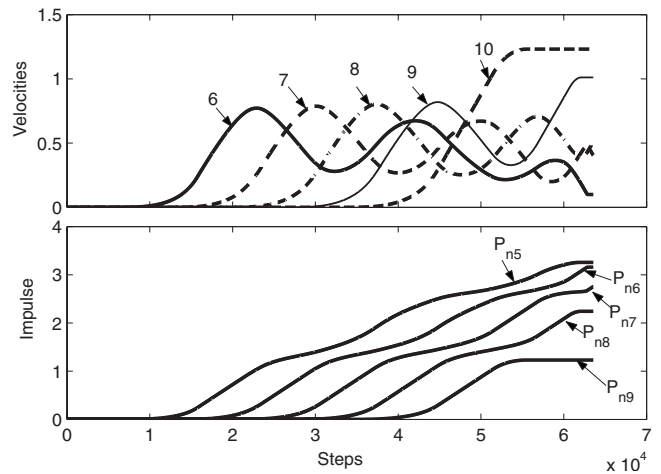

FIG. 16. The evolutions of the velocities and the normal impulses for a chain with seven particles impacted by 3 balls: $\beta = 3:7$ (balls 1 to 5).
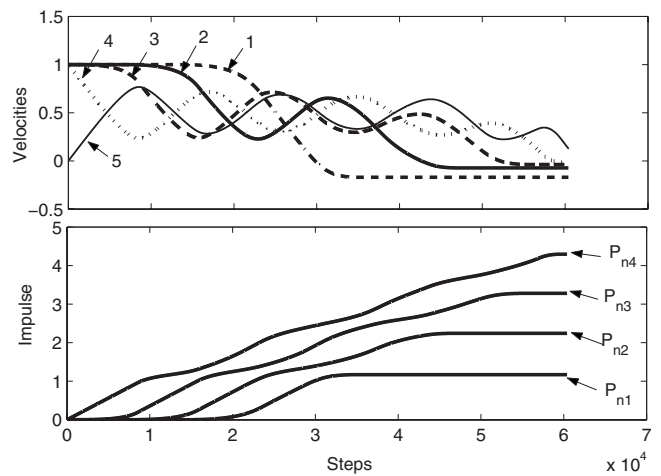

FIG. 18. The evolutions of the velocities and the normal impulses for a chain with six particles impacted by 4 balls: $\beta = 4:6$ (balls 1 to 5).
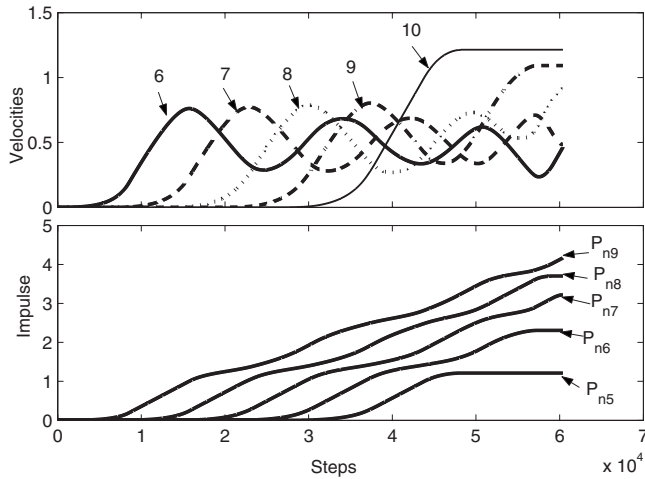
FIG. 19. The evolutions of the velocities and the normal impulses for a chain with six particles impacted by 4 balls: $\beta=4:6$ (ball 6 to 10).

chain impacted by one identical ball. The forward kinetic energy is not concentrated in the last two balls, but will disperse in a length with about four balls.

As m increases, the interactions between the contacts becomes more complex, and the number of balls rebounding backwards decreases. Figures 16 and 17 present the evolutions of the velocities and of the normal impulses for the balls from Nos. 1 to 5 and from Nos. 6 to 10 in the chain with $\beta=3:7$, respectively. Observing the values presented in Table II we can find that the forward kinetic energy changes little, while the number of balls moving forward is five and the kinetic energy is dispersed in a wider scope.

When m increases to four, the postimpact velocity of the last ball changes very little in comparison with the cases of a chain impacted by two balls or three balls, while the forward kinetic energy will disperse in the chain with six balls as shown in Table II. The evolutions of the velocities of each ball and the impulses among various contacts are shown in Figs. 18 and 19.

In conclusion, as m increases, the ratio

$$\frac{\text{(forward postimpact kinetic energy)}}{\text{(total kinetic energy)}} \approx 99\,\%,$$

and the number of balls with a positive postimpact velocity increases as $m+2$. These results confirm that the proposed scheme is able to reproduce the dispersive effects observed for such impacts [8,48].

B. Two solitary waves collision

Collisions between two identical solitary waves traveling in opposite directions are also investigated in the physics community [17,49]. A question to be concerned with herein is whether at the point of intersection, the opposing solitary waves could be annihilated completely, i.e., whether the center of the central grain suffers any motion at any time. Let us set a chain with 15 identical balls that are stationary and keep contact with adjacent balls. The contact relationship between the balls is assumed to be nonlinear elastic and satisfies Hertz assumption (i.e., $\eta=3/2$).

Suppose that two balls with the same velocity, $|v_0|=1$ m/s collide against the ends of this chain from two opposite directions. Two impulsive waves will be generated at the ends of this symmetric structure, and are propagated through the chain (shown in Fig. 20). The five curves correspond to the velocities of the balls at five different instants (different P_j), where the solid line represents the initial condition of the chain, while the other four lines describe the impulsive wave behavior at different times.

Initially the imparting balls at the ends of this chain only influence the adjacent balls with limited length, and then two impulsive waves are formed due to the coupling between adjacent balls (self-organized behaviors among the balls), then travel through the chain with an approximately fixed length and a constant amplitude (similar to a solitary wave). Meanwhile, the balls behind the wave will rebound backwards with small velocities, confirming the scattering phenomenon or bead detachment effect [8]. The length of the
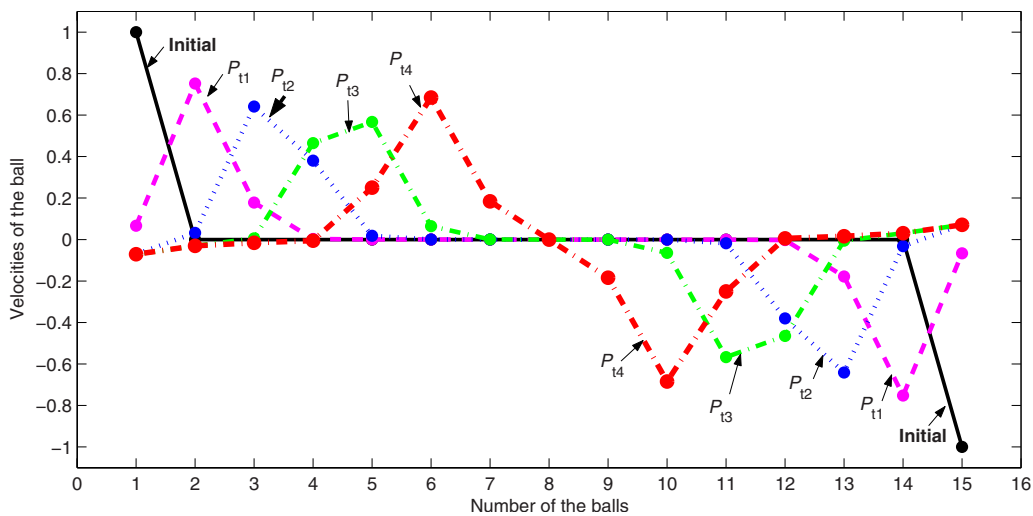

FIG. 20. (Color online) The impulsive wave shape in the 15-ball system at different P_{ti} that represents the different instants scaled by impulse.
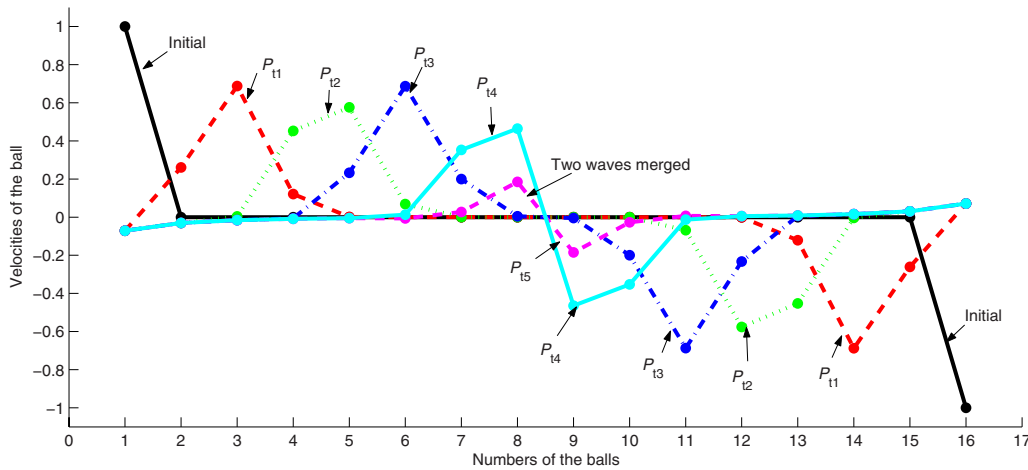
FIG. 21. (Color online) The impulsive wave shape in the 16-ball system at different P_{ti} that represents the different instants scaled by impulse.

impulsive wave is confined in five balls, that well coincides with conclusions obtained from numerical results, theoretical analysis as well as the experiments reported in [9,15,29]. The two impulsive waves originated from the ends of this chain will meet at the chain center, in which the located particle always keeps motionless due to the symmetric structure of the chain. After that, the waves with unchanged shape will reflect from the center of the chain to make particles separate from each other.

If the number of balls in the chain is even, the two impulsive waves will interfere with each other when the waves reach the center of the chain. This phenomenon is well reflected in Fig. 21 obtained by setting the chain with 16 identical balls. When the two waves met at the center of the chain, the velocities of the particles involved in the impulsive wave will abruptly decrease, and thus the momenta resided in particles will be redistributed to form a different shape of wave profiles. However, the variation of the wave profile has little influence on the final outcomes of the velocities after impacts according to our numerical simulation. It is imaginable that the waves will be split or oscillate when the center particle is different from the other ones, and so-called secondary solitary waves will be generated after the two solitary waves meet with one another. These phenomena have been pointed out in [17,49].

V. SUMMARY AND CONCLUSION

The energy of colliding bodies during granular systems will be transferred and redistributed through the network of contact points. Moreover, part of the energy will be dissipated at the vicinity of contacts because of the plastic deformation or other factors. Establishing a model that can clearly separate the dissipation effects and the dispersion of energy among various contacts is crucial for the understanding of the rich and complex behaviors exhibited in granular media.

According to the method proposed in [6], the energetic coefficient seems to be a good candidate in the energy sense to confine the local energy loss, while the dispersion effects should depend on a distributing law that is related to the relative stiffness and the mode of the potential energy accumulation between two particles. This method clearly separates dissipation and dispersion effects during multiple impacts and gives a legible picture for the dynamics of multiple impacts. The comparisons between our numerical predictions and the experimental results in [8] show good agreement, thus validating the proposed algorithm. This method may highlight a way of better understanding the complex phenomena exhibited in granular systems and paves the way to controlling the global behavior through adjusting the microproperties of the particles.

[1] C. Goldenberg, and I. Goldhirsch, Nature (London) **435**, 188 (2005).

[2] I. S. Aranson and Lev S. Tsimring, Rev. Mod. Phys. **78**, 641 (2006).

[3] M. V. Hecke, Science **317**, 49 (2007).

[4] V. Narayan, S. Ramaswamy, and N. Menon, Science **317**, 105 (2007).

[5] B. Brogliato, *Nonsmooth Mechanics*, 2nd ed. (Springer, London, 1999).

[6] C. Liu, Z. Zhao, and B. Brogliato, INRIA Research report, 2008 (unpublished), http://hal.inria.fr

[7] C. Coste, E. Falcon, and S. Five, Phys. Rev. E **56**, 6104 (1997).

[8] E. Falcon, C. Laroche, S. Five, and C. Coste, Eur. Phys. J. B **5**,

111 (1998).

[9] V. F. Nesterenko, J. Appl. Mech. Tech. Phys. **5**, 733 (1983).

[10] V. F. Nesterenko, C. Daraio, E. B. Herbold, and S. Jin, Phys. Rev. Lett. **95**, 158702 (2005).

[11] C. Daraio, V. F. Nesterenko, E. B. Herbold, and S. Jin, Phys. Rev. E **72**, 016603 (2005).

[12] C. Daraio and V. F. Nesterenko, Phys. Rev. E **73**, 026612 (2006).

[13] C. Daraio, V. F. Nesterenko, E. B. Herbold, and S. Jin, Phys. Rev. E **73**, 026610 (2006).

[14] E. B. Herbold and V. F. Nesterenko, Phys. Rev. E **75**, 021304 (2007).

[15] S. Job, F. Melo, A. Sokolow, and S. Sen, Phys. Rev. Lett. **94**, 178002 (2005).

[16] S. Job, F. Melo, A. Sokolow, and S. Sen, Granular Matter **10**, 13C20 (2007).

[17] F. S. Manciu and S. Sen, Phys. Rev. E **66**, 016616 (2002).

[18] M. Manciu, S. Sen, and A. J. Hurd, Phys. Rev. E **63**, 016614 (2000).

[19] E. Avalos, J. M. M. Pfannes, T. R. Krishna. Mohan, and S. Sen, Physica D **225**, 211 (2007).

[20] L. Vergara, Phys. Rev. Lett. **95**, 108002 (2005).

[21] S. Luding, E. Clement, A. Blumen, J. Rajchenbach, and J. Duran, Phys. Rev. E **49**, 1634 (1994).

[22] S. Luding, Int. J. Solids Struct. **41**, 5821 (2004).

[23] E. J. Hinch and S. Saint-Jean, Proc. R. Soc. London, Ser. A **455**, 3201 (1999).

[24] E. Hascoet and E. J. Hinch, Phys. Rev. E **66**, 011307 (2002).

[25] A. Rosas and K. Lindenberg, Phys. Rev. E **68**, 041304 (2003).

[26] A. Rosas and K. Lindenberg, Phys. Rev. E **69**, 037601 (2004).

[27] J. Hong, Phys. Rev. Lett. **94**, 108001 (2005).

[28] J. Hong, J.-Y. Ji, and H. Kim, Phys. Rev. Lett. **82**, 3058 (1999).

[29] W. Ma, C. Liu, B. Chen, and L. Huang, Phys. Rev. E **74**, 046602 (2006).

[30] P. J. Wang, J. H. Xia, Y. D. Li, and C. S. Liu, Phys. Rev. E **76**, 041305 (2007).

[31] S. Luding, Granular Matter **10**(4), 235 (2008).

[32] T. S. Majmudar, M. Sperl, S. Luding, and R. P. Behringer, Phys. Rev. Lett. **98**, 058001 (2007).

[33] S. Luding, E. Clement, A. Blumen, J. Rajchenbach, and J. Duran, Phys. Rev. E **50**, R1762 (1994).

[34] S. McNamara and E. Falcon, Phys. Rev. E **71**, 031302 (2005).

[35] S. McNamara and E. Falcon, Powder Technol. **182**, 232 (2008).

[36] I. S. Aranson, D. Volfson, and L. S. Tsimring, Phys. Rev. E **75**, 051301 (2007).

[37] D. Volfson, A. Kudrolli, and L. S. Tsimring, Phys. Rev. E **70**, 051312 (2004).

[38] I. S. Aranson and L. S. Tsimring, Phys. Rev. E **67**, 021305 (2003).

[39] H. S. Wright, M. R. Swift, and P. J. King, Phys. Rev. E **74**, 061309 (2006).

[40] M. Ramaioli, L. Pournin, and Th. M. Liebling, Phys. Rev. E **76**, 021304 (2007).

[41] J. Crassous, D. Beladjine, and A. Valance, Phys. Rev. Lett. **99**, 248001 (2007).

[42] N. V. Brilliantov, F. Spahn, J. M. Hertzsch, and T. Poschel, Phys. Rev. E **53**, 5382 (1996).

[43] W. J. Stronge, *Impact Mechanics* (Cambridge University Press, Cambridge, 2000).

[44] H. Lankarani and P. Nikravesh, Nonlinear Dyn. **5**, 193 (1994).

[45] E. Hairer and G. Wanner, *Solving Ordinary Differential Equations II. Stiff and Differential-Algebraic Problems*, 2nd ed. Springer Series in Computational Mathematics Vol. 14 (Springer-Verlag, Berlin, 1996).

[46] F. Pfeiffer and Ch. Glocker, *Multibody Dynamics with Unilateral Contacts*, Wiley Series in Nonlinear Science (Wiley, New York, 1996).

[47] M. H. Sadd, Q. Tai, and A. Shukla, Int. J. Non-Linear Mech. **28**, no. 2, 251 (1993).

[48] S. Luding, E. Clément, A. Blumen, J. Rajchenbach, and J. Duran, Phys. Rev. E **50**, 4113 (1994).

[49] S. Sen, M. Manciu, R. S. Sinkovits, and A. J. Hurd, Granular Matter **3**, 33C39 (2001).